

One-Step Synthesis of Core-Shell-Structured Mixed-Metal CPO-27(Cu,Co) and Investigations on Its Controlled Thermal Transformation

Johannes Bitzer,^[a] Christoph Göbel,^[b] Ayas Muhamad Ismail,^[a] Qi Fu,^[b] Martin Muhler,^[b] and Wolfgang Kleist^{*[a, c]}

Using the mixed-metal approach, a direct synthesis route at ambient pressure was developed for a new type of bimetallic metal-organic framework based on the CPO-27 structure. The structural characterization of CPO-27(Cu_{0.6}–CS–Co_{0.4}) using X-ray diffraction, transmission electron microscopy, energy-dispersive X-ray mapping and X-ray absorption spectroscopy revealed that the Cu²⁺ and Co²⁺ ions were exclusively incorporated at the metal positions of the CPO-27 lattice, but with a core-shell distribution within the crystallites. The parent framework material was then utilized as a precursor for the generation of novel bimetallic carbon-supported materials using the controlled thermal decomposition in a reducing atmosphere. During this decomposition process, the distribution of the two metals remained the same, which resulted in unique needle-shaped particles with a high dispersion of cobalt at the periphery of the amorphous carbon and agglomerated copper particles in the inside.

The honeycomb-like CPO-27 (also known as MOF-74) structure is built from divalent metal centers and 2,5-dioxido-terephthalate linker molecules (cf. Figure 1).^[1] In the solvated state, each metal ion is octahedrally coordinated by five oxygen atoms from the linker molecules and one oxygen from a solvent molecule. Various metals have been used for the formation of the CPO-27 structure (e.g. Co^[1], Ni^[2], Zn^[3], Cu^[4], Fe^[5], Mg^[6], Mn^[7]). Apart from monometallic CPO-27 structures, several bi-^[8]

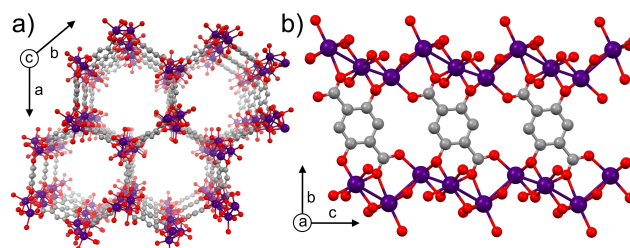


Figure 1. Schematic representation of the CPO-27 structure along the *c* axis (a) and perpendicular to the *c* axis (b) showing the coordination of the metal ions and linker molecules within the structure. Metals: purple; O: red; C: gray; H: omitted.

or even multimetallic^[9] CPO-27 materials have been reported, in which the metals were claimed to be statistically distributed within the framework structure. In particular, the metal combination Cu/Co was reported by Fu *et al.*^[8c] and Orcajo *et al.*^[8d] and the resulting materials were used as a catalyst for the aerobic oxidation of styrene or hydrogen adsorption, respectively. Furthermore, Cai *et al.* also used the Co/Cu combination for the synthesis of a core-shell structured CPO-27 material in a two-step procedure.^[10] In a similar fashion, a core-shell structured mixed-metal CPO-27 material with the metal combination Co/Ni was reported.^[11]

The concept of isostructural mixed-metal metal-organic framework materials, in which all metals are distributed over crystallographically equivalent framework position, is easy to realize when metals with similar properties (e.g. size, electronegativity, preferred coordination environment) are combined.^[12] However, depending on the synthesis conditions and the combination of metals, different structural arrangements of the metal ions within the lattice can be obtained.^[12a] In the majority of multimetallic metal-organic framework (MOF) materials, a statistical distribution of all metal ions is targeted, which enables a straightforward tailoring of properties. However, in recent years, metal-organic frameworks with a core-shell distribution of two metals have increasingly been investigated.^[12a,c,13] The intentional separation of both metals can result in unprecedented and unique properties that cannot be obtained otherwise.

Such materials are often synthesized in a two-step procedure, in which the core material is obtained first and subsequently used as a seed for the formation of the shell. Direct synthesis procedures are still comparatively rare,

[a] Dr. J. Bitzer, A. Muhamad Ismail, Prof. Dr. W. Kleist
Faculty of Chemistry and Biochemistry
Industrial Chemistry – Nanostructured Catalyst Materials
Ruhr University Bochum
Universitätsstraße 150, 44801 Bochum, Germany

[b] Dr. C. Göbel, Dr. Q. Fu, Prof. Dr. M. Muhler
Faculty of Chemistry and Biochemistry
Laboratory of Industrial Chemistry
Ruhr University Bochum
Universitätsstraße 150, 44801 Bochum, Germany

[c] Prof. Dr. W. Kleist
Department of Chemistry – Technical Chemistry
TU Kaiserslautern
Erwin-Schrödinger-Straße 54, 67663 Kaiserslautern, Germany
E-mail: kleist@chemie.uni-kl.de
www.chemie.uni-kl.de/kleist

Supporting information for this article is available on the WWW under <https://doi.org/10.1002/ejic.202100227>

© 2021 The Authors. European Journal of Inorganic Chemistry published by Wiley-VCH GmbH. This is an open access article under the terms of the Creative Commons Attribution License, which permits use, distribution and reproduction in any medium, provided the original work is properly cited.

although they are beneficial with respect to sustainability and large-scale production.^[12a,c,13]

We have developed a one-pot synthesis procedure to prepare a mixed-metal CPO-27(Cu_{0.6}CS–Co_{0.4}), in which both metals are distributed in a core-shell fashion within the framework. For this purpose, we have slightly modified a synthesis procedure reported by Fu *et al.*^[8c] and performed the synthesis at ambient pressure under reflux cooling. The resulting material contained Co and Cu with a ratio close to the one that was used during synthesis (Cu:Co = 64:36, ICP-OES).

The formation of the CPO-27 structure was confirmed by powder X-ray diffraction (XRD, see Figure S1). No additional reflections of crystalline oxidic or metallic phases were found. A line profile fit assuming the presence of only one CPO-27 phase resulted in a reasonable agreement with the experimental pattern (Figure S2a). However, a closer look on the difference curve indicated that a second phase with low crystallinity might be present, since broad reflections at $2\theta = 16.9$, 21.9 and 25.8° could not be fitted. Indeed, a second profile fit with the assumption of two separate CPO-27 phases resulted in a better agreement with the experimental data (Figure S2b). As starting values, the structure parameters of the corresponding monometallic CPO-27 materials were used. The derived unit cell parameters of both fitted phases (Table S1) were compared to literature values of CPO-27(Cu) and CPO-27(Co) materials. Based on the significant metal dependence of the *c* parameter, the two phases were assigned to CPO-27(Cu) (major component with narrow reflections) and CPO-27(Co) (minor component with broad reflections, cf. Figure S2c). Therefore, a statistical distribution of both metals within the CPO-27 structure did not seem plausible.

The IR spectra showed a stronger similarity to CPO-27(Cu) than to CPO-27(Co) (see Figure S4). However, the band centered at 1249 cm^{-1} showed a shift relative to the corresponding bands of CPO-27(Cu) (1252 cm^{-1}) and CPO-27(Co) (1239 cm^{-1}), which was initially expected to occur for a statistical distribution of both metal centers. Nitrogen physisorption measurements (see Figure S6 and Table S2) showed that the synthesized mixed-metal material featured pores in the micropore regime and a specific surface area of $S_{\text{BET}} = 740\text{ m}^2/\text{g}$ was determined. X-ray absorption spectra (see Figure S7 and Figure S8) of CPO-27(Cu_{0.6}CS–Co_{0.4}) at the K-edges of Co and Cu were similar to

monometallic CPO-27(Co) and CPO-27(Cu), respectively. However, significant differences in the intensity of the shells were visible in the Fourier-transformed EXAFS spectra for shells with $R > 2\text{ \AA}$ at both edges (see Figure S8, no phase shift correction was applied). These differences might be attributed to small structural distortions around the metal centers. Due to the complexity of the local structure in combination with this mixed-metal system, no structure fitting based on the Fourier-transformed EXAFS spectra was possible. Furthermore, no conclusive statement on the distribution of cobalt and copper in the framework structure was possible based on data obtained with XRD and X-ray absorption spectroscopy (XAS).

Transmission electron microscopy (TEM) measurements (see Figure 2b and Figure 2c) showed that needle-shaped crystallites of different sizes were formed during the synthesis of CPO-27(Cu_{0.6}CS–Co_{0.4}). No larger agglomerates of metallic or oxidic particles were visible in the recorded images. Energy-dispersive X-ray mapping (EDX) was used to investigate the metal arrangement within the crystallites and a core-shell distribution of both metals was found (see Figure 2a and Figure 2d). The obtained images clearly showed that Cu was present in the center and Co in the shell within the needle-shaped crystallites. The measured XRD pattern is in good accordance with the electron microscopy/EDX measurements, since narrow reflections are expected for the comparatively thick Cu-containing core. Furthermore, the thinner Co-containing shell should result in significantly broader reflections. Consequently, bulk CPO-27(Cu) was formed in the beginning of the synthesis and, subsequently, the surface was covered with CPO-27(Co) resulting in the observed core-shell arrangement. This arrangement results from different crystallization rates of the CPO-27 structure depending on the metal at the used synthesis conditions. Such a behavior has been observed before for other metal-organic framework structures,^[14] but is usually difficult to predict and to control.

Furthermore, neither particles with a statistical metal distribution nor a physical mixture of two monometallic CPO-27 particles were observed in the EDX images. An earlier report of a bimetallic CPO-27 material also claimed a core-shell distribution of both metals, but in that work, cobalt was present in the core and copper in the shell of the crystallites and, thus, opposite to our present study.^[10]

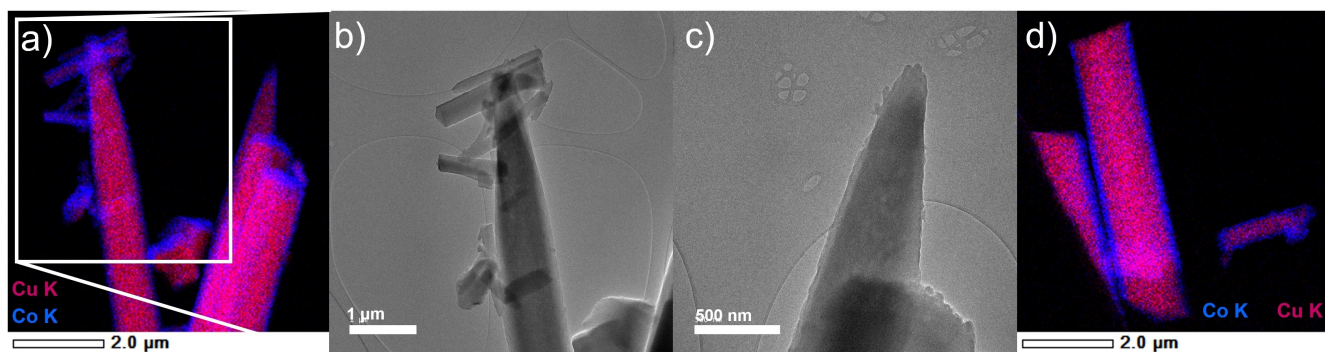


Figure 2. Transmission electron microscopy (TEM; b, c) and energy-dispersive X-ray mapping (EDX; a, d) images of CPO-27(Cu_{0.6}CS–Co_{0.4}).

Since we have successfully obtained this metal-organic framework material with core-shell distribution of both metals, we also wanted to test whether the metal distribution would remain intact during the controlled thermal decomposition. Furthermore, we wanted to investigate how both metals would behave during such thermal treatments.

The controlled thermal decomposition of metal-organic framework materials, also known as MOF-mediated synthesis (MOFMS), has gained growing attention in electrochemistry^[15] and heterogeneous catalysis^[16] within recent years. For the MOFMS, an initially synthesized MOF material is used as sacrificial template, which can be converted either into metal oxides or into carbon-based materials depending on the applied conditions. One of the main benefits of MOFMS for the development of carbon-based materials is the structure-templating effect. In several cases, the morphology and the distribution of metals from the MOF template is retained during MOFMS and can, therefore, be used to tailor the properties of carbon materials in a new manner. The thermal decomposition of MOF materials at elevated temperatures in inert or reducing atmospheres is one of the commonly used routes applied in MOFMS.^[15–17] During the transformation process, the metal centers are partially or completely reduced and the linker molecules are converted into an amorphous or graphitic carbon matrix, in which the newly formed and often highly dispersed metal particles are embedded. The thermal decomposition of monometallic as well as mixed-metal CPO-27 has been reported for applications as highly active catalyst materials^[89,10,18] or supercapacitors^[8h].

Thermogravimetric measurements of CPO-27(Cu_{0.6}-CS-Co_{0.4}) (see Figure S10) either in pure He or in 20% H₂/He showed a first weight loss below 200 °C, which may be attributed to the removal of solvent molecules from the pores. The highest weight-loss rates were observed at 272 °C (H₂/He) and 372 °C (He), respectively. The higher residual mass in He atmosphere may be explained by the presence of a larger amount of oxygen and carbon in the residue after the thermal decomposition. Based on these results, the pristine CPO-27(Cu_{0.6}-CS-Co_{0.4}) material was used for the thermal decomposition in a reducing atmosphere (20% H₂/He) at 300 °C and 400 °C for 1 h, respectively. These temperatures should guarantee that the CPO-27 structure is partially destroyed, but the organic linkers are not fully converted into gaseous compounds, thus, resulting in a residual carbon matrix after the treatment. The thermal decomposition resulted in a color change from deep red to black, which already indicated that the framework structure was destroyed at the applied temperatures. Instead of reflections from the CPO-27 structure, intense reflections at 43.5, 50.5, 74.2° in the XRD patterns confirmed the formation of metallic Cu particles at both temperatures (see Figure S3). Furthermore, a broad reflection of presumably Cu₂O was observed at 37.5°. A size approximation of the Cu particles by using the Scherrer equation for the reflection at 2θ=43.5° resulted in crystallite sizes of 14 nm and 22 nm for 300 °C and 400 °C, respectively. The ratio of Cu and Co did not change significantly during the decomposition procedure (ICP-OES: 61:39 at 300 °C, 65:35 at 400 °C).

The ATR-IR spectra (see Figure S5) showed that several of the bands of CPO-27(Cu_{0.6}-CS-Co_{0.4}) were also visible for the pyrolyzed materials, but their intensity was lower, and the bands were broadened. These observations indicate that an amorphous carbon-based matrix with some structural similarities to CPO-27 seems to be present after the treatments. The nitrogen uptake decreased strongly resulting in low specific surface areas of 70 m²/g and 50 m²/g after pyrolysis at 300 °C and 400 °C, respectively (see Figure S6 and Table S2). Such a drastic decrease of the specific surface area was expected, due to the collapse of the large hexagonal pores of the CPO-27 structure during the thermal transformation. Furthermore, the micropore analysis (t-plot method) suggested that the determined surface areas result only from the external surface and not from the presence of micropores.

X-ray absorption spectra were recorded to determine the oxidation state of both metals before and after the thermal decomposition. The XANES spectra (see Figure 3a and Figure 3b) showed that the 2+ oxidation state of Co remained nearly unchanged after decomposition at 300 °C, whereas the majority of the Cu centers were reduced. The reduced intensity of the white line at the Cu K-edge and the similarity to a reference Cu foil were conclusive indications thereof. These observations are in agreement with the XRD patterns showing

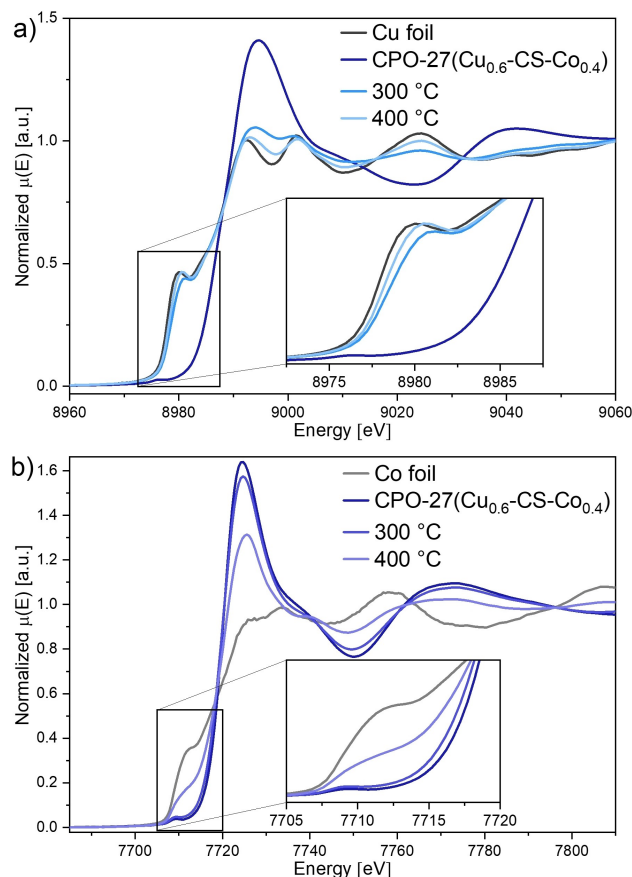


Figure 3. XANES spectra of CPO-27(Cu_{0.6}-CS-Co_{0.4}) in comparison to the thermally decomposed materials recorded at the K-edges of Cu (a) and Co (b).

the presence of metallic Cu particles. The Cu centers were slightly more reduced after the thermal decomposition at 400 °C. Furthermore, also a significant number of Co centers were found in a reduced state, since the intensity of the white line decreased, the edge shifted to lower energies and the formation of a shoulder similar to metallic Co was observed. However, the absence of reflections of metallic Co in the XRD patterns after treatment at 400 °C indicated that the reduced Co centers seemed to be well dispersed in the form of small particles. Due to the noble character of Cu in comparison to Co, it was reasonable that the Cu centers were reduced first.

The observations in the EXAFS and Fourier-transformed EXAFS spectra at the Cu K-edge (see Figure S9b+d) support these assumptions. The spectra of the decomposed materials were more similar to the Cu foil than pristine CPO-27(Cu_{0.6}–CS–Co_{0.4}). While the material before pyrolysis showed the presence of a shell at 1.55 Å (note that no phase shift correction was applied) belonging to 6 nearest oxygen back-scatterers in the framework structure, this shell was not visible for both thermally decomposed materials. However, a new shell at 2.25 Å was visible, which was identified as Cu back-scatterers from metallic Cu particles, since this shell is also observed with strong intensity in the Fourier-transformed EXAFS spectrum of a reference Cu foil.

The intensity of this shell increased with increasing decomposition temperature. On the one hand, an increased fraction of Cu⁰, which has been observed in the XANES spectra, can lead to an increased intensity. On the other hand, the sintering of particles at higher temperatures can also lead to an increased intensity of this shell, because the ratio of surface-to-bulk atoms decreases with increasing particle size. Indeed, an increased particle size of the Cu particles was observed at 400 °C compared to 300 °C in the XRD patterns.

The Fourier-transformed EXAFS spectra at the Co K-edge (see Figure S9c) showed that the local environment of the Co centers after thermal decomposition at 300 °C differed only slightly from the pristine state. The main difference was visible as a slightly reduced intensity of the first shell at 1.6 Å (nearest oxygen neighbors). After decomposition at 400 °C, the partial reduction of Co centers resulted in a significantly lower intensity at this distance, but a contribution of a shell of oxygen

neighbors at 1.6 Å would still be expected in the Fourier-transformed EXAFS spectrum for residual Co²⁺ centers. Such a shell may be present as shoulder but could not clearly be identified in the measured spectrum. Furthermore, a shell at 2.1 Å was visible only at 400 °C, which matched with the distance of Co back-scatterers in metallic Co particles. The intensity of this shell was small compared to the Co foil, which is in agreement with the formation of small Co particles within the carbon matrix. Also, the presence of dispersed Co²⁺ cations is expected to be partially responsible for this low intensity. The comparison to reference spectra suggested that cobalt oxides cannot be found in both materials after the thermal treatment.

TEM and EDX images (Figure 4) showed that the needle shape of the particles was retained during the decomposition process and that Cu was present in the inside and Co close to the surface of the needles. As assumed above, Co was well dispersed and no larger particles were observed after the thermal decomposition at 300 °C and 400 °C, whereas Cu was aggregated to larger particles. The number of these Cu particles within the needles seemed to be lower and their size increased at 400 °C compared to 300 °C due to sintering. The electron microscopy images showed that a broad Cu particle size distribution was present.

SEM images (see Figure S11 and Figure S12) showed that the surface of the needles was smooth without any holes on the observed length scale. In particular, no or only few Cu particles were found at the outer surface. These observations confirm that the formed Cu particles are only present within the needles.

Although earlier publications also reported on the synthesis of core-shell structured Cu–Co particles,^[19] the present approach represents an elegant way for the synthesis of larger core-shell structures, which is not restricted to a single metallic particle, but allows for the generation of multiple nanoparticles within a defined nanostructure.

In summary, the direct synthesis of mixed-metal CPO-27(Cu_{0.6}–CS–Co_{0.4}) resulted in needle-shaped crystallites, in which both metals were distributed in a core-shell fashion with Cu in the core and Co in the shell of the CPO-27 structure. The thermal decomposition of this material in a reducing atmosphere at 300 °C and 400 °C resulted in unprecedented core-

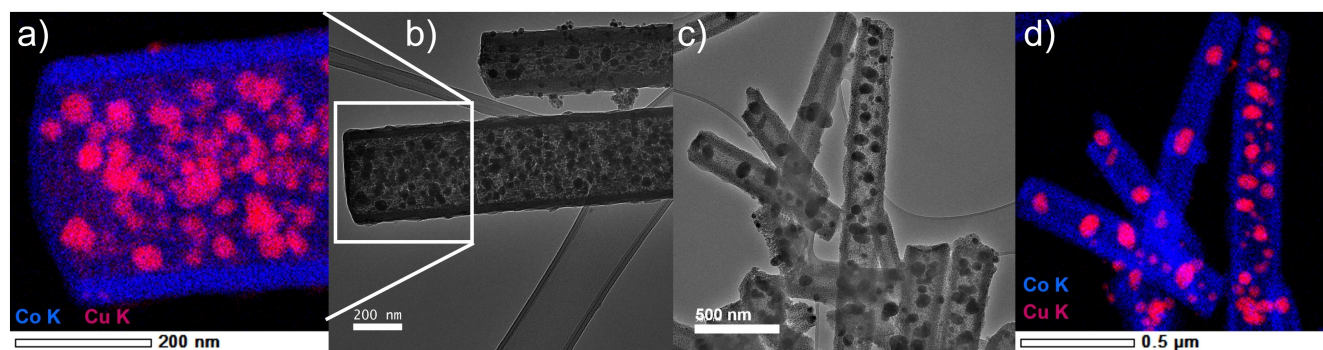


Figure 4. TEM (b+c) and EDX mapping (a,d) images of CPO-27(Cu_{0.6}–CS–Co_{0.4}) after thermal decomposition in 20% H₂/He atmosphere at 300 °C (a,b) and 400 °C (c,d).

shell-structured, needle-shaped particles, in which metallic Cu particles are present within a Co/carbon shell, as derived from TEM, SEM and EDX mapping images. XAS showed that Cu was already present mainly in the metallic state after the decomposition at 300 °C, while Co was only partially reduced even at 400 °C. These novel materials are promising for future applications as heterogeneous catalysts, as electrocatalysts, or because of their magnetic properties, since they might show unique properties due to the arrangement both metals.

Acknowledgements

J. Bitzer thanks the Evangelisches Studienwerk Villigst e.V. for financial support. We acknowledge DESY (Hamburg, Germany), a member of the Helmholtz Association HGF, for the provision of experimental facilities. Parts of this research were carried out at PETRA III and we would like to thank Dr. Edmund Welter for assistance in using beamline P65 (proposal I-20191191). Prof. Ute Krämer and Petra Dücking are acknowledged for performing the ICP-OES measurements and Hartmut Mammen for performing the XRD measurements. Open access funding enabled and organized by Projekt DEAL.

Conflict of Interest

The authors declare no conflict of interest.

Keywords: Metal-organic frameworks · Mixed-metals · Nanostructures · Template synthesis · Thermal decomposition

- [1] P. D. C. Dietzel, Y. Morita, R. Blom, H. Fjellvåg, *Angew. Chem. Int. Ed.* **2005**, *44*, 6354–6358; *Angew. Chem.* **2005**, *117*, 6512–6516.
 [2] P. D. C. Dietzel, B. Panella, M. Hirscher, R. Blom, H. Fjellvåg, *Chem. Commun.* **2006**, 959–961.
 [3] N. L. Rosi, J. Kim, M. Eddaoudi, B. Chen, M. O’Keeffe, O. M. Yaghi, *J. Am. Chem. Soc.* **2005**, *127*, 1504–1518.
 [4] R. Sanz, F. Martínez, G. Orcajo, L. Wojtas, D. Briones, *Dalton Trans.* **2013**, *42*, 2392–2398.
 [5] M. März, R. E. Johnsen, P. D. C. Dietzel, H. Fjellvåg, *Microporous Mesoporous Mater.* **2012**, *157*, 62–74.

- [6] P. D. C. Dietzel, R. Blom, H. Fjellvåg, *Eur. J. Inorg. Chem.* **2008**, *2008*, 3624–3632.
 [7] W. Zhou, H. Wu, T. Yildirim, *J. Am. Chem. Soc.* **2008**, *130*, 15268–15269.
 [8] a) D. Kim, A. Coskun, *Angew. Chem. Int. Ed.* **2017**, *56*, 5071–5076; *Angew. Chem.* **2017**, *129*, 5153–5158; b) S. Chen, M. Xue, Y. Li, Y. Pan, L. Zhu, S. Qiu, *J. Mater. Chem. A* **2015**, *3*, 20145–20152; c) Y. Fu, L. Xu, H. Shen, H. Yang, F. Zhang, W. Zhu, M. Fan, *Chem. Eng. J.* **2016**, *299*, 135–141; d) G. Orcajo, J. A. Villajos, C. Martos, J. Á. Botas, G. Calleja, *Adsorption* **2015**, *21*, 589–595; e) J. A. Botas, G. Calleja, M. Sánchez-Sánchez, M. G. Orcajo, *Int. J. Hydrogen Energy* **2011**, *36*, 10834–10844; f) G. Ayoub, B. Karadeniz, A. J. Howarth, O. K. Farha, I. Đilović, L. S. Germann, R. E. Dinnebier, K. Užarević, T. Friščić, *Chem. Mater.* **2019**, *31*, 5494–5501; g) B. N. Bhadra, S. H. Jung, *Nanoscale* **2018**, *10*, 15035–15047; h) C. Young, J. Kim, Y. V. Kaneti, Y. Yamauchi, *ACS Appl. Mater. Interfaces* **2018**, *1*, 2007–2015; i) Y. Qiao, Y. Ni, F. Kong, R. Li, C. Zhang, A. Kong, Y. Shan, *Chem. Asian J.* **2019**, *14*, 2676–2684.
 [9] L. J. Wang, H. Deng, H. Furukawa, F. Gándara, K. E. Cordova, D. Peri, O. M. Yaghi, *Inorg. Chem.* **2014**, *53*, 5881–5883.
 [10] J. Cai, Y. Zhuang, Y. Chen, L. Xiao, Y. Zhao, X. Jiang, L. Hou, Z. Li, *ChemCatChem* **2020**, *12*, 6241–6247.
 [11] H. Li, F. Yue, H. Xie, C. Yang, Y. Zhang, L. Zhang, J. Wang, *CrystEngComm* **2018**, *20*, 889–895.
 [12] a) J. Bitzer, W. Kleist, *Chem. Eur. J.* **2019**, *25*, 1866–1882; b) S. Abednatanzi, P. Gohari Derakhshandeh, H. Depauw, F.-X. Coudert, H. Vrielinck, P. van der Voort, K. Leus, *Chem. Soc. Rev.* **2019**, *48*, 2535–2565; c) M. Y. Masoomi, A. Morsali, A. Dhakshinamoorthy, H. Garcia, *Angew. Chem. Int. Ed.* **2019**, *58*, 15188–15205; *Angew. Chem.* **2019**, *131*, 15330–15347.
 [13] L. Feng, K.-Y. Wang, G. S. Day, H.-C. Zhou, *Chem. Soc. Rev.* **2019**, *48*, 4823–4853.
 [14] a) C. G. Carson, J. Ward, X. T. Liu, J. Schwartz, R. A. Gerhardt, R. Tannenbaum, *J. Phys. Chem. C* **2012**, *116*, 15322–15328; b) H. Depauw, I. Nevjestic, J. de Winne, G. Wang, K. Haestraete, K. Leus, A. Verberckmoes, C. Detavernier, F. Callens, E. de Canck, H. Vrielinck, P. van der Voort, *Chem. Commun.* **2017**, *53*, 8478–8481.
 [15] W. Xia, A. Mahmood, R. Zou, Q. Xu, *Energy Environ. Sci.* **2015**, *8*, 1837–1866.
 [16] L. Oar-Arteta, T. Wezendonk, X. Sun, F. Kapteijn, J. Gascon, *Mater. Chem. Front.* **2017**, *1*, 1709–1745.
 [17] A. Aijaz, J. Masa, C. Rösler, W. Xia, P. Weide, A. J. R. Botz, R. A. Fischer, W. Schuhmann, M. Muhler, *Angew. Chem. Int. Ed.* **2016**, *55*, 4087–4091; *Angew. Chem.* **2016**, *128*, 4155–4160.
 [18] a) J. Cai, Y. Li, M. Zhang, Z. Li, *Inorg. Chem.* **2019**, *58*, 7997–8002; b) D. Sun, L. Ye, F. Sun, H. García, Z. Li, *Inorg. Chem.* **2017**, *56*, 5203–5209.
 [19] a) Y. Du, N. Cao, L. Yang, W. Luo, G. Cheng, *New J. Chem.* **2013**, *37*, 3035; b) W. Gao, Y. Zhao, H. Chen, H. Chen, Y. Li, S. He, Y. Zhang, M. Wei, D. G. Evans, X. Duan, *Green Chem.* **2015**, *17*, 1525–1534.

Manuscript received: March 18, 2021

Revised manuscript received: April 26, 2021

Accepted manuscript online: April 30, 2021